Letter

Ripples of the QCD critical point

Wei-jie Fu,[1] Xiaofeng Luo,[2] Jan M. Pawlowski,[3,4] Fabian Rennecke,[5,6] and Shi Yin[1,*]

[1]*School of Physics, Dalian University of Technology, Dalian 116024, People's Republic of China*
[2]*Key Laboratory of Quark & Lepton Physics (MOE) and Institute of Particle Physics, Central China Normal University, Wuhan 430079, People's Republic of China*
[3]*Institut für Theoretische Physik, Universität Heidelberg, Philosophenweg 16, 69120 Heidelberg, Germany*
[4]*ExtreMe Matter Institute EMMI, GSI, Planckstraße 1, D-64291 Darmstadt, Germany*
[5]*Institut für Theoretische Physik, Justus-Liebig-Universität Gießen, 35392 Gießen, Germany*
[6]*Helmholtz Research Academy Hesse for FAIR, Campus Gießen, 35392 Gießen, Germany*

(Received 30 September 2023; accepted 21 January 2025; published 10 February 2025)

We investigate the impact of a critical end point (CEP) on the experimentally accessible baryon-number fluctuations of different orders. By now, its potential location has been constrained fairly accurately within first principles functional QCD, together with the location of the chiral crossover line and further thermodynamic observables. This information is incorporated in an advanced QCD-assisted low-energy effective theory which is used for the computation of baryon-number fluctuations at the chemical freeze-out. This computation also takes care of global baryon-number conservation at larger density, where the system changes from grand-canonical to canonical statistics. We observe a prominent peak structure, whose amplitude depends on the location of the CEP, while its position is more sensitive to the location of the freeze-out curve. Our results provide guidance for future low-energy heavy-ion experiments.

DOI: 10.1103/PhysRevD.111.L031502

Introduction. At low densities QCD undergoes a thermal crossover from a deconfined, chirally symmetric high temperature phase to the hadronic phase with confinement and dynamical chiral symmetry breaking at low temperatures. This transition is by now well understood both experimentally and theoretically. In turn, at high densities this simple crossover behavior either ends in a critical end point (CEP) or in a different phase, e.g., with spatial modulations [1–4]. Since it is characterized by the onset of qualitatively different behavior, we refer to the region where this happens as *onset regime*. Locating this regime and studying its properties via its imprints at chemical freeze-out provides the most efficient way to unveil the mysteries of the QCD phase diagram at finite temperature and high baryon densities [5,6].

This onset regime at high densities casts an observable shadow at lower densities: *In the critical regime* close to a CEP, fluctuations of conserved charges show a sizable nonmonotonic behavior due to universal scaling, see e.g. [7–13]. It has been shown in [14], that a sizable nonmonotonic behavior is even seen *far outside the critical regime* dominated by universal scaling. Its origin in this noncritical regime is the successive sharpening of the chiral crossover. Importantly, the details of this sharpening encode the location of the onset regime as ripples in water encode that of the stone causing them. Hence, an in-detail analysis of both experimental measurements and theoretical computations of the observables even far away from this regime can be used to predict or reconstruct its location. This is facilitated due to the emergence of soft (light) modes with a significantly increased correlation length even outside the critical regime [15].

Remarkably, a nonmonotonic variation in the kurtosis of net-proton number distributions has recently been observed by the STAR Collaboration with 3.1σ significance in the first phase of the Beam Energy Scan program at the Relativistic Heavy Ion Collider (RHIC) [10]. The kurtosis of proton distributions at the collision energy $\sqrt{s_{\rm NN}} = 3$ GeV in the fixed-target experiment is consistent with the hadronic results [16,17], suggesting that a potential CEP is located in a region related to a collision energy above 3 GeV.

This is compatible with converged estimates from first-principles functional QCD studies with the functional renormalization group (fRG) and Dyson-Schwinger equations: the location of the onset regime is constrained by $600\ \text{MeV} \lesssim \mu_{B_{\rm CEP}} \lesssim 650\ \text{MeV}$, see [2,18–20], and therefore in range of fixed-target experiments.

*Contact author: yinshi2014@mail.dlut.edu.cn

A combined in-detail analysis of experimental data and theoretical results opens a path towards pinning down the location and properties of the onset regime. This requires the systematic theoretical study of the physics specific to heavy-ion collisions at lower beam energies as well as their imprints in the experimental data. For that purpose we construct an advanced low-energy effective theory (LEFT) based on state-of-the-art functional QCD results. In this LEFT, the onset is signaled by a CEP. This setup allows us to unravel experimental imprints of a CEP within baryon-number fluctuations at freeze-out. We find a prominent peak structure, whose amplitude depends on the location of the CEP, while its position is more sensitive to the location of the freeze-out curve. In summary, the present approach provides, for the first time, quantitative access to the CEP and its properties.

Functional QCD at finite temperature and density. The phase structure of QCD can be resolved with functional QCD approaches through the nonperturbative computation of QCD correlation functions. These correlation functions allow for the determination of observables such as critical temperatures, condensates and conserved charge distributions. Importantly, computations at finite density are not obstructed by the sign problem as for lattice QCD, and are only limited by the computational resources required for computations in reliable approximations. By now functional QCD can access the regime with $\mu_B/T \lesssim 4$ with quantitative precision, and allows for qualitative estimates in the regime $\mu_B/T \gtrsim 4$. For recent reviews see [21–23].

These functional QCD studies have passed through strict benchmark tests in the regime of $\mu_B/T \lesssim 2$–3, where the respective results on the phase structure and on fluctuations can be compared with results from lattice QCD simulations, see e.g. [24–30] and the recent review [31]. Hence, they represent themselves a self-consistent analytic continuation from QCD with $\mu_B/T \lesssim 3$. Accordingly, results from functional QCD at $\mu_B/T \gtrsim 3$ are not only fully compatible with constraints from analytic extrapolations based on lattice data, see e.g. [31–34], their reliability qualitatively surpasses that of analytic extrapolations as they are based on solving dynamical equations in QCD.

The present fRG approach with a QCD-assisted LEFT relies on results and technical advances in the description of first-principles QCD at finite temperature and density with the fRG put forward in [2], based on [35–42] in the vacuum and at finite temperature. The construction of a quantitatively reliable LEFT is facilitated by the fact that the glue dynamics decouple very efficiently due to the gluonic mass gap of QCD at energy scales of about 1 GeV [2,22,23]. This entails that low-energy QCD is well described by the respective emergent LEFT: QCD without gluonic fluctuations but in a gluonic background. Moreover, quantitative precision is then obtained by using the fRG to match the RG flows of QCD to those of the LEFT. This setup has been named *QCD-assisted LEFT*, and a first study including a detailed discussion of the setup has been presented in [14].

In the present work we aim for quantitative precision and reliable predictions at high densities. This is achieved by directly evolving the RG flow of quark-meson scattering processes obtained in first-principles QCD in [2] in our LEFT. These processes encode the correlations between quarks and gluons in the channel that carries the dynamics of the chiral condensate. This allows us to accurately capture the CEP as it arises in QCD at large μ_B, while being in excellent agreement with lattice data at small μ_B. The CEP in the present QCD-assisted LEFT is located at

$$(T_{\mathrm{CEP}}, \mu_{B_{\mathrm{CEP}}}) = (98, 643)\ \mathrm{MeV}, \tag{1}$$

consistent with the constraint

$$600\ \mathrm{MeV} \lesssim \mu_{B\mathrm{CEP}} \lesssim 650\ \mathrm{MeV}, \tag{2}$$

in full functional QCD [2,18–20]. Equation (2) is the state-of-the-art uncertainty estimate for the location of CEP from functional QCD. Variations of the CEP location within this regime are possible and we shall use them later for an investigation of the experimental imprints and properties of the regime around the CEP. The details of our setup can be found in the supplement.

Baryon number fluctuations at freeze-out. In the present work we use vanishing chemical potentials for the electric charge and strangeness, as the effects of the corresponding charge conservation are subleading for baryon-number fluctuations [43–45]. We thus compute the grand potential $\Omega[T, \mu_B]$ and extract from it the pressure,

$$p = -\Omega[T, \mu_B], \tag{3}$$

and the generalized susceptibilities,

$$\chi_n^B = \frac{\partial^n}{\partial(\mu_B/T)^n}\frac{p}{T^4}. \tag{4}$$

The χ_n^B are directly related to the cumulants of the net-baryon-number distribution, whose proxy, the net-proton distribution, can be measured in the experiments [46]. The cumulants of the lowest four orders, the mean value M, the variance σ, the skewness S and the kurtosis κ, are given by

$$\frac{M}{VT^3} = \chi_1^B, \qquad \frac{\sigma^2}{VT^3} = \chi_2^B, \qquad S = \frac{\chi_3^B}{\chi_2^B \sigma}, \qquad \kappa = \frac{\chi_4^B}{\chi_2^B \sigma^2}, \tag{5}$$

where we have already divided out the volume dependence. The latter is naturally absent in the ratio between two susceptibilities of different orders,

$$R^B_{nm} = \frac{\chi^B_n}{\chi^B_m}. \tag{6}$$

These ratios have been computed in equilibrium and at vanishing density in lattice QCD, e.g. [29,47–49] and with functional methods both at vanishing and finite density, e.g. [14,50–54].

In particular in the regime of low collision energy, high-order baryon-number fluctuations are significantly suppressed by global baryon-number conservation, [55–57]. In order to accurately describe the relevant features of the medium created in heavy-ion collisions, this is taken into account here by considering canonical corrections to grand canonical susceptibilities. To this end, we adopt the subensemble acceptance method (SAM) as proposed in [56]. In SAM the ratio between the subensemble volume, V_1, measured in the acceptance window and that of the whole system, V, is given by $\alpha = V_1/V$. In the thermodynamic limit, where both sizes of total- and subsystems are significantly larger than the correlation length ξ, the measured cumulants in the subsystem approach the grand canonical values discussed above when $\alpha \to 0$. When the effect of global baryon-number conservation begins to play a role, the parameter α develops a nonzero value and canonical corrections apply.

We fix α with the most sensitive and well-observed ratio of low-order fluctuations. This is R_{32}, for which the experimental data show a significant flattening for $\sqrt{s_{\rm NN}} \lesssim 11.5$ GeV which is not seen in R_{32} computed within the grand canonical ensemble. We attribute a sizable part of it to the increasing importance of canonical statistics and use the discrepancy to fix α. Notably, there are further effects such as the detector acceptance [9] and volume fluctuations [58]. They are considered to be subleading in the present work. The difference between the net-proton and net-baryon fluctuations is discussed in detail in the Supplemental Material [59], where one can find that this difference can also be partially accounted for by our choice of α.

In Fig. 1 we depict our theoretical results and the experimental measurements for R_{32}. Our results are shown both without and with canonical corrections. Evidently, for $\sqrt{s_{\rm NN}} \gtrsim 11.5$ GeV, the effects of global baryon-number conservation are negligible and we use $\alpha = 0$ in this range. For $\sqrt{s_{\rm NN}} \lesssim 11.5$ GeV the importance of global baryon-number conservation increases. The qualitative behavior is well captured with a linear dependence of the parameter α on $\sqrt{s_{\rm NN}}$, to wit,

$$\alpha(\bar{s}) = a(1 - \sqrt{\bar{s}})\theta(1 - \bar{s}), \tag{7a}$$

with the Heaviside θ function and the parameters

$$a = 0.33, \qquad \sqrt{\bar{s}} = \frac{\sqrt{s_{\rm NN}}}{11.9\ \text{GeV}}. \tag{7b}$$

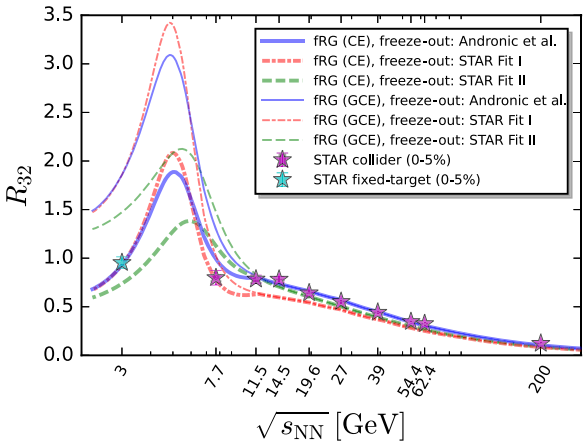

FIG. 1. Ratio R_{32} of baryon-number fluctuations defined in (6) for the grand-canonical ensemble (GCE) and with canonical corrections at small beam energies due to global baryon-number conservation (CE). The latter are taken into account with SAM [56] and fixed using STAR data from Refs. [10,11,16]. Three different freeze-out curves are used [14].

The parameters are obtained by matching our results with the experimental data at three different energies. We find $\alpha = 0$ at $\sqrt{s_{\rm NN}} = 11.5$ GeV, $\alpha = 0.14$ at $\sqrt{s_{\rm NN}} = 7.7$ GeV, and $\alpha = 0.24$ at $\sqrt{s_{\rm NN}} = 3$ GeV. Fitting these points yields the parameters in (7). More details are provided in the Supplemental Material [59].

Finally, we use three different freeze-out curves introduced in our previous work [14]: The first one is obtained through a parametrization of the freeze-out data from [60]; the others are based on the data from the STAR experiment [61] and are denoted by STAR Fit I and STAR Fit II. In STAR Fit I, all the freeze-out data from STAR are used in the fit. In STAR Fit II some collision energy data are dropped, considered to be flawed from general considerations. For more details on the fitting procedure see [14].

Results for baryon number fluctuations. With our setup in place, we can investigate further fluctuation observables. In Fig. 2 we show the ratios of baryon-number fluctuations R^B_{21}, R^B_{32}, R^B_{42}, R^B_{51}, R^B_{62} with canonical corrections as functions of the collision energy for the three different freeze-out curves mentioned above. Our results are compared with experimental measurements by the STAR Collaboration, including the ratio between the variance and mean value R^p_{21}, skewness R^p_{32}, kurtosis R^p_{42} of net-proton distributions for central (0%–5%) Au + Au collisions [10], fifth- and sixth-order net-proton fluctuations R^p_{51}, R^p_{62} with centrality 0%–40% [62], proton cumulants in fixed-target collisions at $\sqrt{s_{\rm NN}} = 3$ GeV [16].

In general, Fig. 2 shows that our results are in very good agreement with the experimental data, keeping in mind the caveats of directly comparing conserved charge and net-proton fluctuations [9,64,65]. For R_{21} we see a small

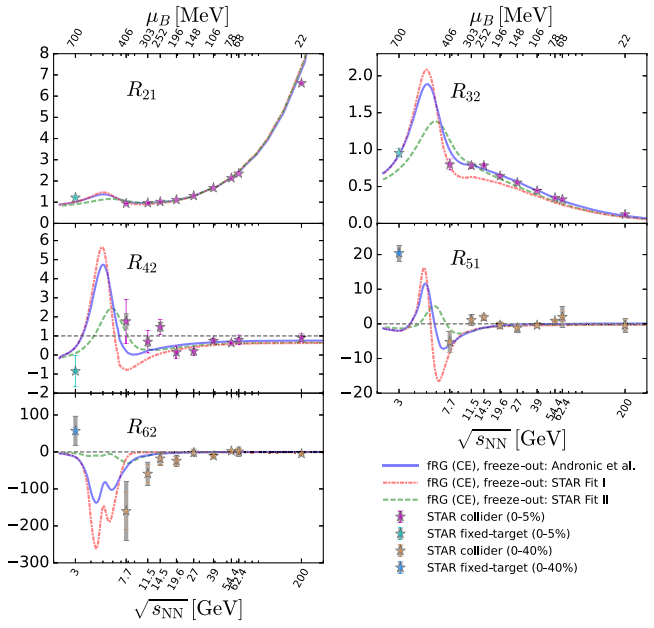

FIG. 2. Baryon-number fluctuations of different orders as functions of the collision energy, calculated in the QCD-assisted LEFT with the fRG on three different freeze-out curves [14], where the effects of global baryon-number conservation are taken into account in the range of $\sqrt{s_{\rm NN}} \lesssim 11.5$ GeV through SAM [56], see text for more details. Experimental data measured by STAR are also presented for comparison [10,11,16,62,63].

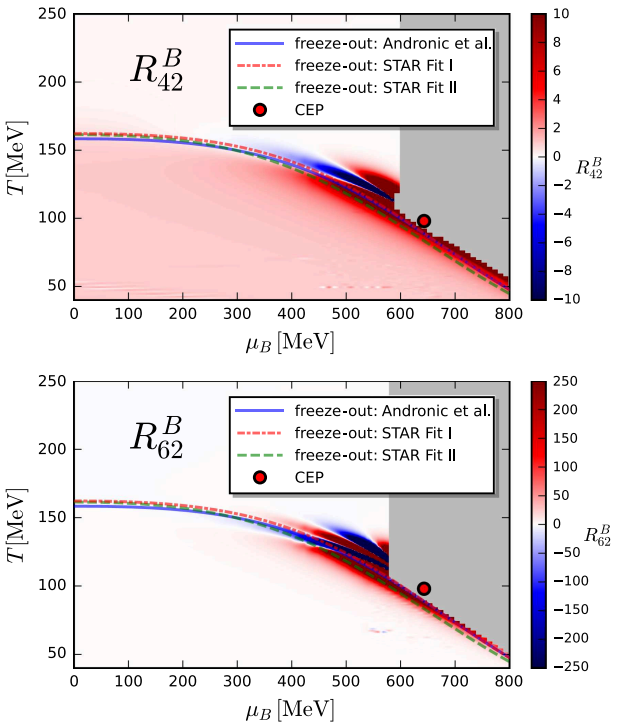

FIG. 3. Heat map of R^B_{42} (top) and R^B_{62} (bottom) in a grand canonical ensemble in the phase diagram obtained in the QCD-assisted LEFT within the fRG with a CEP located at $(T_{\rm CEP}, \mu_{B_{\rm CEP}}) = (98, 643)$ MeV, where three different freeze-out curves are depicted [14]. The gray area depicts the region where the computation of R^B_{42} or R^B_{62} is inaccessible within the present numerical setup.

deviation at the highest collision energy $\sqrt{s_{\rm NN}} = 200$ GeV. This can be attributed to a slight mismatch in the freeze-out chemical potentials at this beam energy, namely, $\mu_{B\rm CF} \simeq 22$ MeV in theory and $\mu_{B\rm CF} \simeq 27$ MeV in experiment [61]. R^p_{42} is perhaps the most prominent experimental observable used in the search for the CEP in the QCD phase diagram. The significant nonmonotonic behavior for 7.7 GeV $\leq \sqrt{s_{\rm NN}} \leq 200$ GeV observed by STAR [10] is also seen in our results. For the hyperorder fluctuations R^B_{51} and R^B_{62} we find that the fRG results are qualitatively consistent with experimental data with $\sqrt{s_{\rm NN}} \gtrsim 7.7$ GeV, where both R^B_{51} and R^B_{62} develop negative values with decreasing collision energy. In comparison to the grand canonical results presented in the Supplemental Material [59], one finds that the magnitudes of high-order fluctuations, especially the hyperorder ones, are suppressed considerably in the regime of low collision energy. Note that both values of R^B_{62} and R^B_{51} at $\sqrt{s_{\rm NN}} = 3$ GeV are negative, which seems to be inconsistent with experimental data. However, their data is taken at 0%–40% centrality [62], while our theoretical description is not geared towards off-central collisions.

A common feature of all observables shown in Fig. 2 is a pronounced peak structure between 3 and 7.7 GeV. These peaks appear to be quite sensitive to the choice of freeze-out curve. Additional experimental data in this region would therefore greatly constrain the location of the freeze-out curve at small beam energies. Still, this peak is present for all freeze-out curves and, as shown in the Supplemental Material [59], persists under a variation of the location of the CEP.

The connection between the cumulants in the phase diagram and the freeze-out can be read off from Fig. 3, where we show the phase diagram of the QCD-assisted LEFT together with a heat map of R^B_{42} (top panel) and R^B_{62} (bottom panel) in the plane. One can clearly see that the nonmonotonic beam-energy dependence of these ratios and the peak structure both arise from the freeze-out line crossing through positive and negative regions for the ratios. These regions are concentrated in a narrow region around the chiral crossover and more pronounced they become, the sharper the crossover is. For example, the nonmonotonic behavior and the peak structure of R^B_{42} for $\sqrt{s_{\rm NN}} \lesssim 7.7$ GeV can be explained by the freeze-out curve moving away from the transition line, thus it deviates from the negative region and crosses over the lower positive region. The freeze-out baryon chemical potentials of the peak are around 536, 541 and 486 MeV for the freeze-out curves Andronic *et al.*, STAR Fit I and STAR Fit II, respectively. Hence, they are at significantly smaller chemical potentials than the location of the CEP at $\mu_{B_{\rm CEP}} = 643$ MeV. However, the crossover is already quite

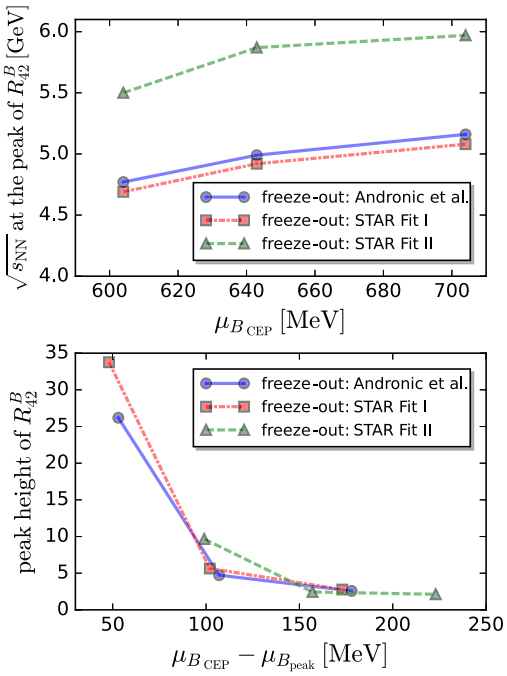

FIG. 4. Top: dependence of the position of the peak in R^B_{42} on the location of the CEP and the freeze-out curve [14]. Bottom: height of the peak in R^B_{42} as a function of the difference between the $\mu_{B_{\rm CEP}}$ and $\mu_{B\rm peak}$, where the latter corresponds to μ_B related to the $\sqrt{s_{\rm NN}}$ of the peak in R^B_{42}.

sharp at these chemical potentials, which leads to large amplitudes of the ratios and hence pronounced peaks.

These findings beg the question as to what determines the height and position of the peak. This can be analyzed by varying the location of the CEP in the QCD-assisted LEFT within the uncertainty band in full functional QCD in (2). We use setups with CEPs at $(T_{\rm CEP}, \mu_{B_{\rm CEP}}) = (108, 604)$ MeV and at (94,704) MeV, and investigate the imprints of this variation on the susceptibilities. The underlying procedure is detailed in the Supplemental Material [59]. We find that the position of the peak, i.e., the beam energy $\sqrt{s_{\rm NN}}$ at the peak in R^B_{42}, is rather insensitive to the location of the CEP, and only depends on the freeze-out curve, see the top panel of Fig. 4. In order to reduce the uncertainty of the freeze-out curve, in the bottom panel of Fig. 4 we depict the height of the peak as a function of $\mu_{B_{\rm CEP}} - \mu_{B\rm peak}$, where $\mu_{B\rm peak}$ is the chemical potential related to $\sqrt{s_{\rm NN}}$ of the peak. The results of three different freeze-out curves almost fall into one single curve. Most importantly, the closer the CEP is to the peak, the higher it is. For $\mu_{B_{\rm CEP}} - \mu_{B\rm peak} \lesssim 100$ MeV, the peak height increases significantly. In short, the information on the location of the CEP is predominantly encoded in the peak height.

Conclusions and summary. In the present work we have presented a satisfactory description of the experimentally measured baryon-number fluctuations. In particular, we predict a characteristic peak structure between beam energies of 3 and 7.7 GeV. The peak can be traced back to a sharpening of the chiral crossover with increasing chemical potential, which is a solid prediction of functional methods [2,18–20].

Our main finding is that the height of this peak is sensitive to the location of the CEP, while its location depends on the details of the freeze-out. The latter occurs in a regime where the R^B_{nm} considered here show no sign of critical scaling. Hence the freeze-out happens outside the universal scaling regime of the CEP in terms of these observables. This has the important implication that our predictions are not affected by nonequilibrium effects that arise from critical slowing down [66,67]. However, since the height of the peak in the kurtosis carries sensitive information on the location of the CEP, the ripples of the CEP can be used to infer its location without the need to rely on critical scaling.

Note that the present setup can also accommodate more general scenarios for the onset regime in future investigations. In these scenarios the crossover may end in a spatially modulated regime and not a CEP, e.g. a moat regime [2–4] or even an inhomogeneous phase [1,68], whose detection asks for even more experimental precision data.

A more quantitative in-detail analysis with the present combined experimental-theoretical approach will allow us to answer both, the question of the precise location of the onset regime and its properties. The success of the endeavor of unraveling the QCD phase structure at high baryon densities requires experimental precision data in this regime, which highlights the importance and discovery potential of future heavy-ion experiments.

Acknowledgments. We thank the members of the fQCD Collaboration [69] for discussions and collaborations on related projects. This work is funded by the National Natural Science Foundation of China under Grants No. 12175030, No. 12122505, No. 11890711, and the National Key Research and Development Program of China under Contracts No. 2022YFA1604900, No. 2020YFE0202002, No. 2018YFE0205201, and the Deutsche Forschungsgemeinschaft (DFG, German Research Foundation) under Germany's Excellence Strategy EXC 2181/1–390900948 (the Heidelberg STRUCTURES Excellence Cluster) and the Collaborative Research Centre SFB 1225–273811115 (ISOQUANT), and the Collaborative Research Centre TransRegio CRC-TR 211"Strong-interaction matter under extreme conditions"—Project No. 315477589—TRR 211.

[1] K. Fukushima and T. Hatsuda, The phase diagram of dense QCD, Rep. Prog. Phys. **74**, 014001 (2011).

[2] W.-j. Fu, J. M. Pawlowski, and F. Rennecke, QCD phase structure at finite temperature and density, Phys. Rev. D **101**, 054032 (2020).

[3] R. D. Pisarski and F. Rennecke, Signatures of moat regimes in heavy-ion collisions, Phys. Rev. Lett. **127**, 152302 (2021).

[4] F. Rennecke, R. D. Pisarski, and D. H. Rischke, Particle interferometry in a moat regime, Phys. Rev. D **107**, 116011 (2023).

[5] M. Arslandok *et al.*, Hot QCD White Paper, arXiv:2303.17254.

[6] *Properties of QCD Matter at High Baryon Density*, edited by X. Luo, Q. Wang, N. Xu, and P. Zhuang (Springer, New York, 2022).

[7] M. A. Stephanov, K. Rajagopal, and E. V. Shuryak, Event-by-event fluctuations in heavy ion collisions and the QCD critical point, Phys. Rev. D **60**, 114028 (1999).

[8] M. Stephanov, Non-Gaussian fluctuations near the QCD critical point, Phys. Rev. Lett. **102**, 032301 (2009).

[9] X. Luo and N. Xu, Search for the QCD critical point with fluctuations of conserved quantities in relativistic heavy-ion collisions at RHIC: An overview, Nucl. Sci. Tech. **28**, 112 (2017).

[10] J. Adam *et al.* (STAR Collaboration), Nonmonotonic energy dependence of net-proton number fluctuations, Phys. Rev. Lett. **126**, 092301 (2021).

[11] M. Abdallah *et al.* (STAR Collaboration), Cumulants and correlation functions of net-proton, proton, and antiproton multiplicity distributions in Au + Au collisions at energies available at the BNL Relativistic Heavy Ion Collider, Phys. Rev. C **104**, 024902 (2021).

[12] D. Mroczek, A. R. Nava Acuna, J. Noronha-Hostler, P. Parotto, C. Ratti, and M. A. Stephanov, Quartic cumulant of baryon number in the presence of a QCD critical point, Phys. Rev. C **103**, 034901 (2021).

[13] T. Dore, J. M. Karthein, I. Long, D. Mroczek, J. Noronha-Hostler, P. Parotto, C. Ratti, and Y. Yamauchi, Critical lensing and kurtosis near a critical point in the QCD phase diagram in and out of equilibrium, Phys. Rev. D **106**, 094024 (2022).

[14] W.-j. Fu, X. Luo, J. M. Pawlowski, F. Rennecke, R. Wen, and S. Yin, Hyper-order baryon number fluctuations at finite temperature and density, Phys. Rev. D **104**, 094047 (2021).

[15] J. Braun *et al.*, Soft modes in hot QCD matter, arXiv:2310.19853.

[16] M. S. Abdallah *et al.* (STAR Collaboration), Measurements of proton high order cumulants in $\sqrt{s_{\mathrm{NN}}} = 3$ GeV Au + Au collisions and implications for the QCD critical point, Phys. Rev. Lett. **128**, 202303 (2022).

[17] M. Abdallah *et al.* (STAR Collaboration), Higher-order cumulants and correlation functions of proton multiplicity distributions in sNN = 3 GeV Au + Au collisions at the RHIC STAR experiment, Phys. Rev. C **107**, 024908 (2023).

[18] F. Gao and J. M. Pawlowski, QCD phase structure from functional methods, Phys. Rev. D **102**, 034027 (2020).

[19] F. Gao and J. M. Pawlowski, Chiral phase structure and critical end point in QCD, Phys. Lett. B **820**, 136584 (2021).

[20] P. J. Gunkel and C. S. Fischer, Locating the critical endpoint of QCD: Mesonic backcoupling effects, Phys. Rev. D **104**, 054022 (2021).

[21] C. S. Fischer, QCD at finite temperature and chemical potential from Dyson–Schwinger equations, Prog. Part. Nucl. Phys. **105**, 1 (2019).

[22] N. Dupuis, L. Canet, A. Eichhorn, W. Metzner, J. M. Pawlowski, M. Tissier, and N. Wschebor, The nonperturbative functional renormalization group and its applications, Phys. Rep. **910**, 1 (2021).

[23] W.-j. Fu, QCD at finite temperature and density within the fRG approach: An overview, Commun. Theor. Phys. **74**, 097304 (2022).

[24] R. Bellwied, S. Borsanyi, Z. Fodor, J. Guenther, S. D. Katz, C. Ratti, and K. K. Szabo, The QCD phase diagram from analytic continuation, Phys. Lett. B **751**, 559 (2015).

[25] A. Bazavov *et al.*, The QCD equation of state to $\mathcal{O}(\mu_B^6)$ from lattice QCD, Phys. Rev. D **95**, 054504 (2017).

[26] A. Bazavov *et al.* (HotQCD Collaboration), Skewness and kurtosis of net baryon-number distributions at small values of the baryon chemical potential, Phys. Rev. D **96**, 074510 (2017).

[27] A. Bazavov *et al.* (HotQCD Collaboration), Chiral crossover in QCD at zero and non-zero chemical potentials, Phys. Lett. B **795**, 15 (2019).

[28] S. Borsanyi, Z. Fodor, J. N. Guenther, S. K. Katz, K. K. Szabo, A. Pasztor, I. Portillo, and C. Ratti, Higher order fluctuations and correlations of conserved charges from lattice QCD, J. High Energy Phys. 10 (2018) 205.

[29] A. Bazavov *et al.*, Skewness, kurtosis, and the fifth and sixth order cumulants of net baryon-number distributions from lattice QCD confront high-statistics STAR data, Phys. Rev. D **101**, 074502 (2020).

[30] D. Bollweg, D. A. Clarke, J. Goswami, O. Kaczmarek, F. Karsch, S. Mukherjee, P. Petreczky, C. Schmidt, and S. Sharma (HotQCD Collaboration), Equation of state and speed of sound of (2 + 1)-flavor QCD in strangeness-neutral matter at nonvanishing net baryon-number density, Phys. Rev. D **108**, 014510 (2023).

[31] G. Aarts *et al.*, Phase transitions in particle physics—results and perspectives from lattice quantum chromo-dynamics, Prog. Part. Nucl. Phys. **133**, 104070 (2023).

[32] S. Mukherjee and V. Skokov, Universality driven analytic structure of the QCD crossover: Radius of convergence in the baryon chemical potential, Phys. Rev. D **103**, L071501 (2021).

[33] D. Bollweg, J. Goswami, O. Kaczmarek, F. Karsch, S. Mukherjee, P. Petreczky, C. Schmidt, and P. Scior (HotQCD Collaboration), Taylor expansions and Padé approximants for cumulants of conserved charge fluctuations at nonvanishing chemical potentials, Phys. Rev. D **105**, 074511 (2022).

[34] S. Borsanyi, Z. Fodor, M. Giordano, J. N. Guenther, S. D. Katz, A. Pasztor, and C. H. Wong, Equation of state of a hot-and-dense quark gluon plasma: Lattice simulations at real μB vs extrapolations, Phys. Rev. D **107**, L091503 (2023).

[35] J. Braun, H. Gies, and J. M. Pawlowski, Quark confinement from color confinement, Phys. Lett. B **684**, 262 (2010).

[36] J. Braun, L. M. Haas, F. Marhauser, and J. M. Pawlowski, Phase structure of two-flavor QCD at finite chemical potential, Phys. Rev. Lett. **106**, 022002 (2011).
[37] M. Mitter, J. M. Pawlowski, and N. Strodthoff, Chiral symmetry breaking in continuum QCD, Phys. Rev. D **91**, 054035 (2015).
[38] J. Braun, L. Fister, J. M. Pawlowski, and F. Rennecke, From quarks and gluons to hadrons: Chiral symmetry breaking in dynamical QCD, Phys. Rev. D **94**, 034016 (2016).
[39] F. Rennecke, Vacuum structure of vector mesons in QCD, Phys. Rev. D **92**, 076012 (2015).
[40] A. K. Cyrol, L. Fister, M. Mitter, J. M. Pawlowski, and N. Strodthoff, Landau gauge Yang-Mills correlation functions, Phys. Rev. D **94**, 054005 (2016).
[41] A. K. Cyrol, M. Mitter, J. M. Pawlowski, and N. Strodthoff, Nonperturbative quark, gluon, and meson correlators of unquenched QCD, Phys. Rev. D **97**, 054006 (2018).
[42] A. K. Cyrol, M. Mitter, J. M. Pawlowski, and N. Strodthoff, Nonperturbative finite-temperature Yang-Mills theory, Phys. Rev. D **97**, 054015 (2018).
[43] W.-j. Fu, J. M. Pawlowski, and F. Rennecke, Strangeness neutrality and QCD thermodynamics, SciPost Phys. Core **2**, 002 (2020).
[44] W.-j. Fu, J. M. Pawlowski, and F. Rennecke, Strangeness neutrality and baryon-strangeness correlations, Phys. Rev. D **100**, 111501 (2019).
[45] R. Wen and W.-j. Fu, Correlations of conserved charges and QCD phase structure, Chin. Phys. C **45**, 044112 (2021).
[46] Y. Hatta and M. A. Stephanov, Proton number fluctuation as a signal of the QCD critical endpoint, Phys. Rev. Lett. **91**, 102003 (2003); **91**, 129901(E) (2003).
[47] A. Bazavov *et al.*, Freeze-out conditions in heavy ion collisions from QCD thermodynamics, Phys. Rev. Lett. **109**, 192302 (2012).
[48] S. Borsanyi, Z. Fodor, S. D. Katz, S. Krieg, C. Ratti, and K. K. Szabo, Freeze-out parameters: Lattice meets experiment, Phys. Rev. Lett. **111**, 062005 (2013).
[49] S. Borsanyi, Z. Fodor, S. D. Katz, S. Krieg, C. Ratti, and K. K. Szabo, Freeze-out parameters from electric charge and baryon number fluctuations: Is there consistency?, Phys. Rev. Lett. **113**, 052301 (2014).
[50] W.-j. Fu and J. M. Pawlowski, Relevance of matter and glue dynamics for baryon number fluctuations, Phys. Rev. D **92**, 116006 (2015).
[51] W.-j. Fu and J. M. Pawlowski, Correlating the skewness and kurtosis of baryon number distributions, Phys. Rev. D **93**, 091501 (2016).
[52] W.-j. Fu, J. M. Pawlowski, F. Rennecke, and B.-J. Schaefer, Baryon number fluctuations at finite temperature and density, Phys. Rev. D **94**, 116020 (2016).
[53] G. A. Almasi, B. Friman, and K. Redlich, Baryon number fluctuations in chiral effective models and their phenomenological implications, Phys. Rev. D **96**, 014027 (2017).
[54] P. Isserstedt, M. Buballa, C. S. Fischer, and P. J. Gunkel, Baryon number fluctuations in the QCD phase diagram from Dyson-Schwinger equations, Phys. Rev. D **100**, 074011 (2019).
[55] A. Bzdak, V. Koch, and V. Skokov, Baryon number conservation and the cumulants of the net proton distribution, Phys. Rev. C **87**, 014901 (2013).
[56] V. Vovchenko, O. Savchuk, R. V. Poberezhnyuk, M. I. Gorenstein, and V. Koch, Connecting fluctuation measurements in heavy-ion collisions with the grand-canonical susceptibilities, Phys. Lett. B **811**, 135868 (2020).
[57] P. Braun-Munzinger, B. Friman, K. Redlich, A. Rustamov, and J. Stachel, Relativistic nuclear collisions: Establishing a non-critical baseline for fluctuation measurements, Nucl. Phys. **A1008**, 122141 (2021).
[58] P. Braun-Munzinger, A. Rustamov, and J. Stachel, Bridging the gap between event-by-event fluctuation measurements and theory predictions in relativistic nuclear collisions, Nucl. Phys. **A960**, 114 (2017).
[59] See Supplemental Material at http://link.aps.org/supplemental/10.1103/PhysRevD.111.L031502 for details of computation and truncation.
[60] A. Andronic, P. Braun-Munzinger, K. Redlich, and J. Stachel, Decoding the phase structure of QCD via particle production at high energy, Nature (London) **561**, 321 (2018).
[61] L. Adamczyk *et al.* (STAR Collaboration), Bulk properties of the medium produced in relativistic heavy-ion collisions from the beam energy scan program, Phys. Rev. C **96**, 044904 (2017).
[62] B. E. Aboona *et al.* (STAR Collaboration), Beam energy dependence of fifth- and sixth-order net-proton number fluctuations in Au + Au collisions at RHIC, Phys. Rev. Lett. **130**, 082301 (2023).
[63] M. Abdallah *et al.* (STAR Collaboration), Measurement of the sixth-order cumulant of net-proton multiplicity distributions in Au + Au collisions at $\sqrt{s_{NN}} = 27$, 54.4, and 200 GeV at RHIC, Phys. Rev. Lett. **127**, 262301 (2021).
[64] A. Bzdak, S. Esumi, V. Koch, J. Liao, M. Stephanov, and N. Xu, Mapping the phases of quantum chromodynamics with beam energy scan, Phys. Rep. **853**, 1 (2020).
[65] V. Vovchenko, V. Koch, and C. Shen, Proton number cumulants and correlation functions in Au-Au collisions at $\sqrt{\mathrm{sNN}} = 7.7$–200 GeV from hydrodynamics, Phys. Rev. C **105**, 014904 (2022).
[66] B. Berdnikov and K. Rajagopal, Slowing out-of-equilibrium near the QCD critical point, Phys. Rev. D **61**, 105017 (2000).
[67] S. Mukherjee, R. Venugopalan, and Y. Yin, Universal off-equilibrium scaling of critical cumulants in the QCD phase diagram, Phys. Rev. Lett. **117**, 222301 (2016).
[68] M. Buballa and S. Carignano, Inhomogeneous chiral condensates, Prog. Part. Nucl. Phys. **81**, 39 (2015).
[69] J. Braun, Y.-r. Chen, W.-j. Fu, F. Gao, F. Ihssen, A. Geissel, J. Horak, C. Huang, J. M. Pawlowski, F. Rennecke, F. Sattler, B. Schallmo, J. Stoll, Y.-y. Tan, S. Töpfel, J. Turnwald, R. Wen, J. Wessely, N. Wink, S. Yin, and N. Zorbach, fQCD Collaboration, (2023).